Journal of Marine Research, 61, 613–634, 2003

The Pacific/Indian Ocean pressure difference and its influence on the Indonesian Seas circulation: Part II—The study with specified sea-surface heights

by Vladimir M. Kamenkovich[1], William H. Burnett[2], Arnold L. Gordon[3] and George L. Mellor[4]

ABSTRACT

In Part II we construct new numerical solutions to further analyze our results in Part I (Burnett *et al.,* 2003), that indicate the lack of a unique relationship between the Pacific/Indian Ocean pressure difference and the total transport of the Indonesian Throughflow (ITF). These new solutions involve perturbations of the sea level relative to the original solutions. We present detailed analyses of the overall momentum and energy balances for these new solutions to stay consistent with the procedures developed in Part I. The results validate our conclusions regarding the lack of a unique relationship between the pressure head and the value of the total transport of the ITF. However, based on results from all the experiments, we have found that the seasonal variations of the total transport of the ITF are in phase with the pressure-head variations. Thus the hypothesis by Wyrtki (1987) that the pressure head, measured by the sea-surface-height difference between Davao (Philippines) and Darwin (Australia), is well correlated with the total transport is qualitatively supported.

1. Introduction

In Part I (Burnett *et al.,* 2003) we discussed the influence of the Pacific-Indian Ocean pressure difference on the Indonesian Seas Throughflow (ITF). We showed strong evidence that external factors—the components of the pressure head (XEPRH and YEPRH) and the local wind stress (WUSURF and WVSURF)— did not uniquely determine the *value* of the total transport of the ITF. Other factors, such as the components of the bottom form stress (XBTS and YBTS), the components of the internal pressure head (XIPRH and YIPRH) and the total inflow and outflow transports caused by the Mindanao Current, North Equatorial Counter Current, and New Guinea Coastal Current were also important (see Appendix A for an explanation of the acronyms).

To derive these conclusions we analyzed the momentum and energy balances for a series

1. Department of Marine Sciences, University of Southern Mississippi, Stennis Space Center, Mississippi, 39529, U.S.A. ***email: vladimir.kamenkovich@usm.edu***
2. Naval Meteorology and Oceanography Command, Stennis Space Center, Mississippi, 39529, U.S.A.
3. Lamont Doherty Earth Observatory of Columbia University, Palisades, New York, 10964, U.S.A.
4. Program in Atmospheric and Oceanic Sciences, Princeton University, Princeton, New Jersey, 08544, U.S.A.

of experiments with prescribed seasonally varying total transports through four open ports (Type I experiments). The *first objective* of Part II is to prove the robustness of these results by performing a series of special experiments with perturbed pressure heads. Then we analyze their impact on the Indonesian Seas circulation pattern and the total transport of the ITF. In these experiments we prescribe seasonally varying sea-surface heights at the open ports rather than the total transports, and we will refer to such experiments as Type II experiments.

The *second objective* of Part II is to analyze whether some relation between seasonal variations of the pressure head and the total transport of the ITF exists or not. Although a unique relation between the pressure head and the total transport of the ITF is lacking, nonetheless a correlation between their seasonal variations could in principle exist. This objective arose from Wyrtki's (1987) hypothesis on the correlation of the pressure head, measured by the sea-surface-height difference between Davao (Philippines) and Darwin (Australia), and the total transport of the ITF. We will address this question by combining the results of the Type I and Type II experiments and analyzing the variations of the different measures of the pressure head.

2. The Type II experiments

In Part I we ran Type I experiments with seasonally varying, normal and tangential velocities prescribed at four open ports. In Part II we will run Type II experiments with the same model configuration but with different boundary conditions by specifying sea-surface heights and tangential velocities at the four open ports (refer to Appendix B for details).

To check the robustness of the results in Part I we consider Type II experiments of a special kind. First, we specify the initial sea-surface height for the Type II experiment, $\eta_{II}^{(i)}$, as the sum of the output of the corresponding annual-mean Type I experiment, $\eta_{I}^{(i)}$, and a sea-surface-height perturbation, η_δ. The perturbation, η_δ, is introduced in the following way. We divide the model domain into the three partitions IO ($0 < I < 45$), IS ($46 < I < 149$), and PO ($150 < I < 250$) shown schematically in Figure 1. Within the IO and PO partitions we specify constant values of $\eta_\delta - \eta_{IO}$ and η_{PO} respectively—while within the IS partition we prescribe a linear interpolation between η_{IO} and η_{PO}. The domain integral of η_δ is then set to zero (the mass conservation constraint) to establish a relation between η_{IO} and η_{PO}. Thus the parameter η_{PO} will be a free variable.

Second, we specify the sea-surface height at the open ports, $\eta_{II}^{(b)}$, as the sum of the output of the seasonally varying Type I experiment at the ports, $\eta_{I}^{(i)}$, and the perturbation η_δ (see the formulation of numerical boundary conditions in Appendix B). The perturbation η_δ does not change in time. Tangential velocities at the ports are taken from the Type I experiment output without any perturbation while, at the closed part of the boundary we specify no-slip boundary conditions. We ramped the model during the first 30 computational days to reduce the impact of transients, and the model reached a seasonally varying

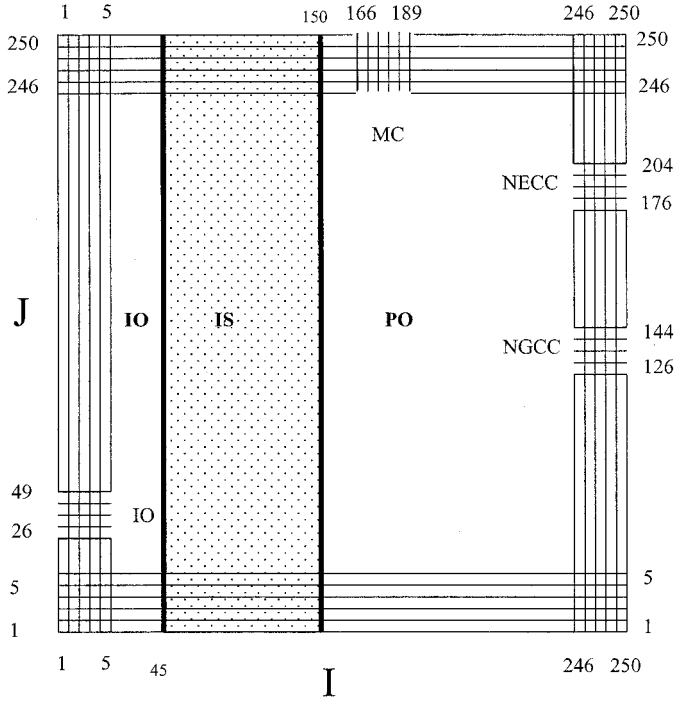

Figure 1. Schematic of the 250 × 250 model domain with the locations of the three partitions IO, IS, and PO.

state within one computational year. Only two computational years of simulation are required for these experiments.

We ran two Type II experiments by setting the sea-surface-height perturbation in the Pacific, η_{PO}, equal to constant value +2.5 mm (Type IIA experiment) or to −2.5 mm (Type IIB experiment) for all seasons. The effect of local winds was not taken into account for these experiments, however we did analyze the effect of local winds in Part I. The Type IIA experiment should increase the pressure head between the two oceans while the Type IIB experiment should decrease the pressure head. Note that the total transport of the ITF is not prescribed for any Type II experiment.

A perturbation of 2.5 mm might seem extremely small for the Indonesian Seas area but this is a barotropic elevation. For a crude estimate of the relation between scales of η in barotropic and baroclinic motions, suppose that the depth-integrated velocities in both models are on the same order. Then, $U_{bc}^{(s)}h \approx U_{bt}H$, (for example, if $U \approx U_{bc}^{(s)} \exp(z/h)$ then $\int_{-H}^{0} U dz \approx U_{bc}^{(s)}h$ since $H \gg h$), where $U_{bc}^{(s)}$ is the typical baroclinic velocity at the sea surface and h is the typical vertical scale for the baroclinic motion; U_{bt} is the typical velocity for a barotropic motion; and H is the depth of the ocean. Thus, $U_{bc}^{s}/U_{bt} \approx H/h$

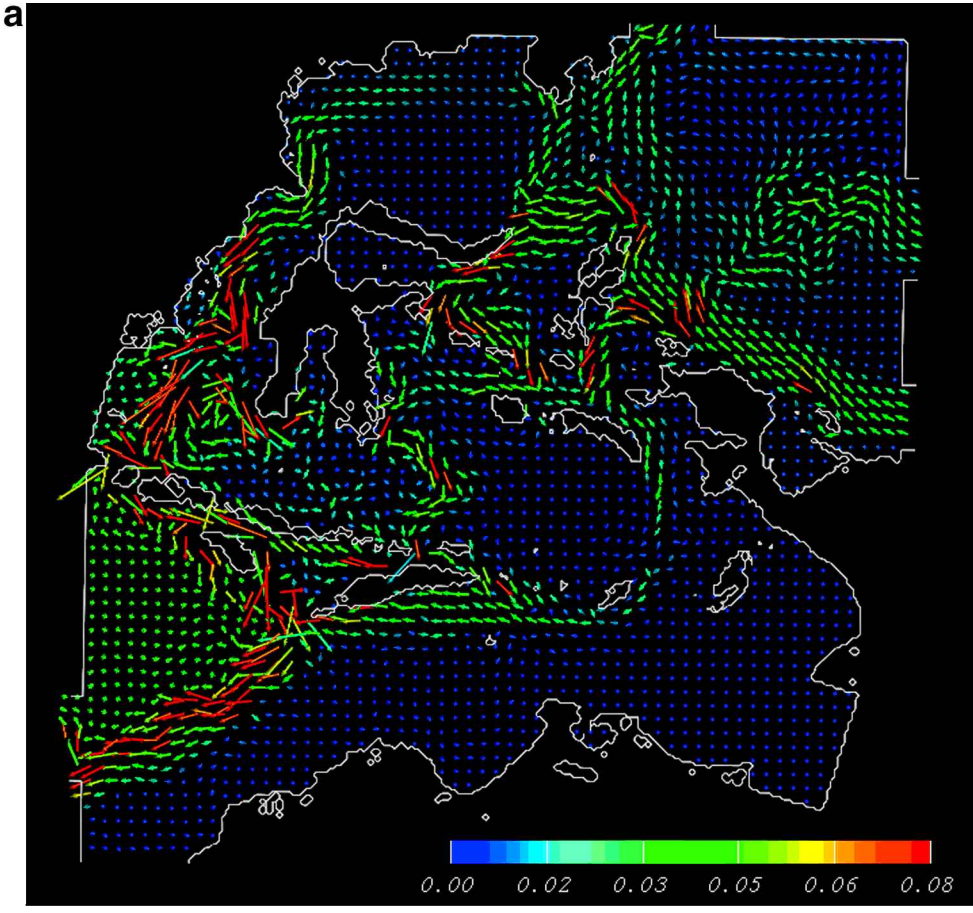

Figure 2. The boreal summer horizontal velocity patterns (m/s) for the Type IIA (a) and IIB (b) experiments.

and from geostrophic relations near the sea surface, it follows that $\eta_{bc}/\eta_{bt} \approx H/h$, where η_{bc} and η_{bt} are the typical values of the sea-surface height for baroclinic and barotropic motions respectively. Finally, if $H/h \sim 10$ then η_{bc}/η_{bt} are also on the order of 10. Therefore, a perturbation of 10 mm in a barotropic model can be considered equivalent to a 10 cm perturbation in a baroclinic model.

The geostrophic relations apply at the four open ports (Burnett *et al.,* 2000; Fig. 1). Therefore, the perturbation, η_δ, in the Type IIA/B experiments was specified in a way that did not change the pressure gradient across the entrances of the open ports. If we succeed in constructing such solutions, we will find circulation patterns with noticeably distinct pressure differences between the Pacific and Indian Ocean, and very small variations in the

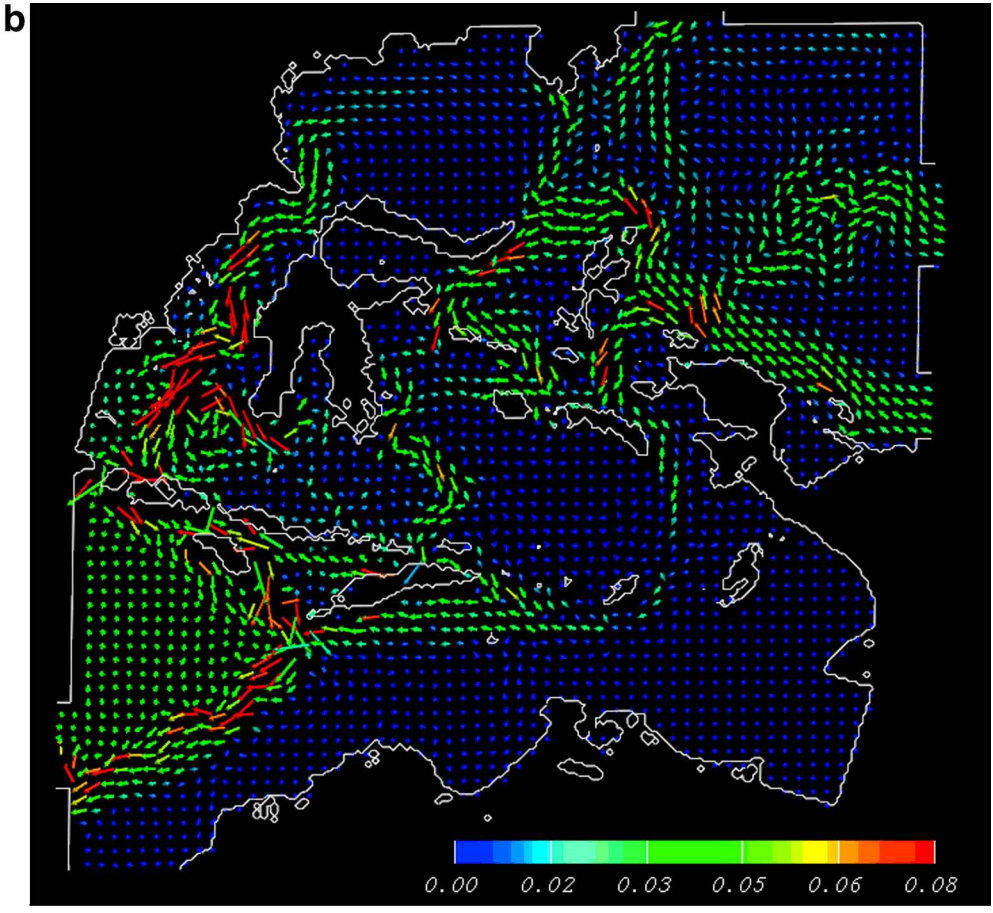

Figure 2. (Continued)

total transports at the open ports. Small variations could be caused by some ageostrophic effects at the open ports, which should be present, for example, due to the placement of the equator near the southern end of the New Guinea Coastal Current (NGCC) port. In Appendix B we further outline the method for constructing Type IIA/B solutions.

Figure 2a,b provide the boreal summer horizontal velocity pattern for the Type IIA and Type IIB experiments, respectively (all seasons discussed in this paper are relative to the Northern Hemisphere), and are representative of other seasons (see Burnett, 2000). The summer total transports through eight selected passageways and four open ports for all experiments are provided in Table 1. The transport through the Indian Ocean open port is the total transport of the ITF. In the Type IIA experiment, the total transport of the ITF increases compared to the Type I experiment, as does the transport through the eight

Table 1. The absolute values of the total transports through the four open ports and eight passages for the Type I and Type IIA/B experiments during summer.

Passage	Type I (Sv)	Type IIA (Sv)	Type IIB (Sv)
Indian Ocean (outflow) or ITF	20.0	22.9	17.9
New Guinea Coastal Current (inflow)	19.0	19.8	18.5
North Equatorial Countercurrent (outflow)	25.0	23.6	25.6
Mindanao Current (inflow)	26.0	26.7	25.0
Makassar Strait (A)	6.4	7.4	5.7
Molucca Sea (B)	10.9	12.6	9.6
Halmahera Sea (C)	3.1	3.4	2.9
Lombok Strait (D)	4.5	5.1	4.1
Sumba Strait (E)	3.6	4.3	3.1
Flores Sea (F)	0.9	1.0	0.7
Ombai Strait (G)	9.4	10.8	8.3
Timor Sea (H)	5.1	5.7	4.6

Refer to Part I, Figure 1 for locations of the ports and passageways.

passageways (labeled A through H in Fig. 1 of Part I). The NECC outflow port is the only open port where the transport through the port is reduced. Throughout the model grid, the horizontal velocity vector magnitudes are larger, however, the velocity directions do not change. Alternatively, for the Type IIB experiment, the total transport of the ITF and the transport through the eight passages decrease. The velocity vectors, throughout the grid, are also smaller and do not change direction.

Figure 3a,b provide the Type II A/B experiment sea-surface heights for the summer (representative of other seasons, see Burnett, 2000). The perturbation of the sea-surface height in the boundary conditions leads to significant changes of the sea-surface height throughout the whole domain. Results from the Type IIA experiment show that higher sea-surface heights occur throughout the Pacific Ocean and lower heights occur in the Indian Ocean, compared to the Type I experiment (see Fig. 6, Part I), qualitatively indicating that the pressure difference increased between the two oceans. Similarly, results from the Type IIB experiment show that lower (higher) sea-surface heights occur throughout the Pacific (Indian Ocean) indicating that the pressure difference decreased between the two oceans. In the next section we will conduct a quantitative analysis of the momentum and energy balances of the Type IIA/B experiments.

3. The momentum and energy balances

In Part I (Burnett *et al.,* 2003) we discussed in detail the overall momentum and energy balances for the series of experiments with the prescribed seasonally varying total transports through the open ports. A similar analysis for the new series of the Type IIA/B

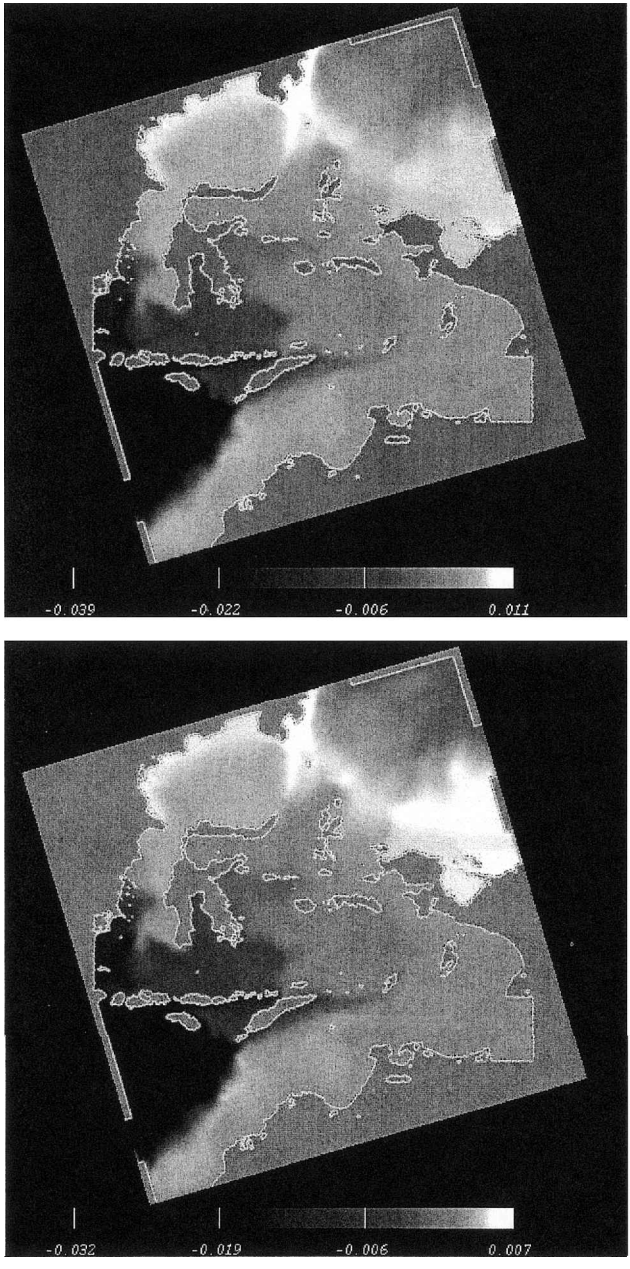

Figure 3. The boreal summer sea surface heights (m) for the Type IIA (a) and IIB (b) experiments.

Table 2. The domain integral x-momentum balance terms for the Type I and Type IIA/B experiments. Refer to Appendix A for the term definitions.

Season (dimensions)	Type	Coriolis (XCOR) $1 \times 10^9 m^4 s^{-2}$	Pressure gradient (XPGRD) $1 \times 10^9 m^4 s^{-2}$	Total pressure head (XPRH) $1 \times 10^9 m^4 s^{-2}$	External pressure head (XEPRH) $1 \times 10^9 m^4 s^{-2}$	Bottom form stress (XBTS) $1 \times 10^9 m^4 s^{-2}$	SSH difference (SSHDIF) $1 \times 10^{-2} m$
Winter	I	0.38×10^{-2}	0.10×10^{-1}	-0.30	-0.29	0.31	-0.96
	IIA	-0.75×10^{-1}	-0.73×10^{-1}	-0.54	-0.54	0.47	-1.47
	IIB	0.79×10^{-1}	0.82×10^{-1}	-0.77×10^{-1}	-0.83×10^{-1}	0.16	-0.46
Spring	I	-0.23	-0.23	-0.97	-0.96	0.74	-2.43
	IIA	-0.31	-0.32	-1.22	-1.21	0.91	-2.98
	IIB	-0.16	-0.17	-0.75	-0.75	0.59	-1.96
Summer	I	-0.45	-0.46	-1.65	-1.64	1.19	-3.97
	IIA	-0.54	-0.55	-1.92	-1.91	1.37	-4.57
	IIB	-0.39	-0.40	-1.44	-1.44	1.05	-3.53
Fall	I	-0.19	-0.19	-0.93	-0.92	0.74	-2.45
	IIA	-0.28	-0.28	-1.19	-1.18	0.92	-3.01
	IIB	-0.13	-0.13	-0.72	-0.72	0.60	-1.98

experiments with the prescribed seasonally varying sea-surface heights at the open ports basically supports the conclusions of Part I. We will briefly review the main results of the experiments without local wind-stress effects. Table 2 provides the overall x-momentum balance terms for each season for the Type I and Type IIA/B experiments. As in Type I experiment the overall x-momentum balance is basically reduced to the overall geostrophic balance:

$$\mathrm{XCOR} = \mathrm{XPGRD}, \tag{1}$$

where, XCOR is the x-component of the Coriolis force and the x-component of the pressure gradient XPGRD is,

$$\mathrm{XPGRD} = \mathrm{XEPRH} + \mathrm{XIPRH} + \mathrm{XBTS}. \tag{2}$$

In our experiments with realistic topography the x-component of the resultant of pressure forces acting on the fluid at the internal side boundaries (XIPRH) appeared negligibly small. The x-component of the resultant of pressure forces acting on the fluid at the external side boundaries (XEPRH) in the experiment IIA is larger than in the experiment IIB. In both experiments, IIA and IIB, the x-component of the bottom form stress (XBTS) is significantly larger than XPGRD, thus stressing the importance of XBTS in determining the total transport of the ITF. Note that the momentum balance terms are at their highest values during the summer, and lowest during the winter, which should be expected since the model highest and lowest transport values occur during the summer and the winter, respectively.

Table 3. The domain integral y-momentum balance terms for the Type I and Type IIA/B experiments. Refer to Appendix A for the term definitions.

Season (dimensions)	Type	Coriolis (YCOR) $1 \times 10^9 m^4 s^{-2}$	Pressure gradient (YPGRD) $1 \times 10^9 m^4 s^{-2}$	Total pressure head (YPRH) $1 \times 10^9 m^4 s^{-2}$	External pressure head (YEPRH) $1 \times 10^9 m^4 s^{-2}$	Bottom form stress (YBTS) $1 \times 10^9 m^4 s^{-2}$
	I	0.43	0.43	0.23	0.20	0.20
Winter	IIA	0.48	0.48	0.16	0.10	0.32
	IIB	0.38	0.38	0.31	0.29	0.71×10^{-1}
	I	0.58	0.57	0.12	0.44×10^{-1}	0.45
Spring	IIA	0.62	0.61	0.45×10^{-1}	-0.53×10^{-1}	0.57
	IIB	0.52	0.52	0.20	0.14	0.32
	I	0.75	0.74	0.42×10^{-1}	-0.81×10^{-1}	0.70
Summer	IIA	0.79	0.78	-0.32×10^{-1}	-0.17	0.81
	IIB	0.69	0.68	0.12	0.19×10^{-1}	0.56
	I	0.62	0.61	0.18	0.10	0.43
Fall	IIA	0.67	0.66	0.11	0.11×10^{-1}	0.55
	IIB	0.57	0.56	0.26	0.20	0.31

The overall geostrophic approximation is valid for the y-momentum balance (see Table 3). Therefore:

$$\text{YCOR} = \text{YPGRD}, \tag{3}$$

where,

$$\text{YPGRD} = \text{YEPRH} + \text{YIPRH} + \text{YBTS}. \tag{4}$$

Contrary to the overall x-momentum balance, the y-component of the resultant of pressure forces acting on the fluid at the internal side boundaries (YIPRH) becomes noticeable. Hence, we find another factor important for determining the total transport of the ITF. As in the x-momentum balance, y-momentum balance terms are at their highest values during the summer, and lowest during the winter.

The overall energy balance terms for the Type I and Type IIA/B experiments are presented in Table 4 for each season. The sum of kinetic and potential energies integrated over the total fluid volume (TENER) for the Type IIA experiment is higher than the corresponding value for the Type I experiment for each season, while TENER for the Type IIB experiment is lower than the corresponding value for the Type I experiment. For all experiments TENER is higher in the summer and lower in the winter, which is expected since the model was developed with the highest transports in the summer and lowest transports in the winter. During each season, the total kinetic energy (the kinetic energy integrated over the total fluid volume) is larger than the total potential energy (approximately by a factor of two or three for the spring, summer, and fall). For all experiments the total work (per unit time) performed by the pressure forces at the four ports (-PREWK) is

Table 4. The domain integral energy balance terms for the Type I and Type IIA/B experiments. Refer to Appendix A for the term definitions.

Season (dimensions)	Type	Kinetic and potential energy sum (TENER) $1 \times 10^9 m^5 s^{-2}$	Work of pressure forces (PREWK) $1 \times 10^6 m^5 s^{-3}$	Work of horizontal friction (HFWK) $1 \times 10^6 m^5 s^{-3}$	Work of bottom friction (BFWK) $1 \times 10^6 m^5 s^{-3}$
	I	1.40	−0.76	−0.72	-0.66×10^{-1}
Winter	IIA	2.31	−1.13	−1.09	−0.14
	IIB	0.90	−0.50	−0.51	-0.38×10^{-1}
	I	4.29	−2.39	−1.88	−0.35
Spring	IIA	6.00	−3.39	−2.59	−0.59
	IIB	3.09	−1.71	−1.38	−0.21
	I	9.68	−5.65	−4.14	−1.19
Summer	IIA	12.29	−7.30	−5.27	−1.69
	IIB	7.99	−4.58	−3.44	−0.89
	I	4.72	−2.49	−2.13	−0.41
Fall	IIA	6.52	−3.46	−2.90	−0.66
	IIB	3.54	−1.79	−1.63	−0.26

basically balanced by the total work (per unit time) performed by the horizontal and bottom friction forces (HFWK and BFWK). So the approximate form of the overall energy balance is

$$\text{PREWK} = \text{HFWK} + \text{BFWK}. \tag{5}$$

In Part I, we performed an additional Type I experiment by setting the bottom depth to a constant value of 4500 m. We found that the bathymetry had a profound influence on the direction and magnitude of the ITF. Analogously we performed a similar Type IIA experiment. Figure 4 shows that the horizontal velocity pattern for the Type II experiment is similar to the Type I experiment, with the ITF flowing along the western boundary, through the Makassar and Lombok Straits, and exiting through the IO open port. The velocity vectors increase in magnitude, compared to the Type I case; however, the vector directions do not change. Therefore, changing the pressure head when the bottom form stress is eliminated does not change the direction of the ITF.

The integral momentum and energy balance relations (1)–(5) are also valid for the constant depth case. When XBTS and YBTS were set to zero, the pressure head, XEPRH, changed by 68% relative to the Type I experiment. The open port transports, Q_{MC}, Q_{NECC}, and Q_{NGCC} changed in the Type IIA experiments, relative to those of the Type I experiment, by approximately 5%; however, for Q_{IO}, the change reached 26%. The transports through the Makassar, Sumba, Ombai Straits, and the Flores and Timor Seas for

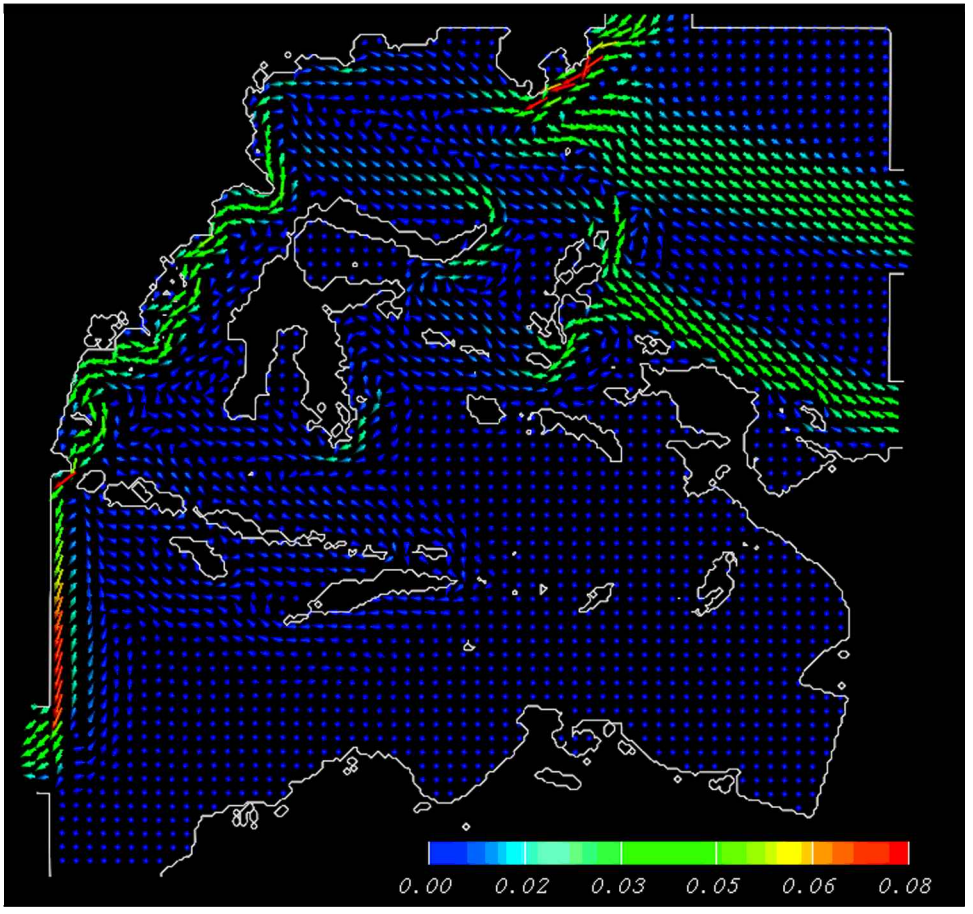

Figure 4. The boreal spring horizontal velocity pattern (m/s) for the Type IIA experiment with $H(\mathrm{I}, \mathrm{J}) = 4500$ m.

the Type IIA experiments changed significantly compared to those of the Type I experiment (on the order of 30%–40%). In the next section we will provide similar estimates for the experiments with the real bottom topography.

Thus the analysis of perturbed solutions (the Type IIA/B experiments) gives the same leading terms in the momentum and energy balances as in the unperturbed solution (the Type I experiment). Therefore, all arguments used in the analysis of the Type I experiment (see Part I) to prove the lack of the unique relation between the pressure heads and the total transport of the ITF are applicable to the Type II experiments as well. In other words, by analyzing the solution of the Type I experiment, we proved, in Part I, the validity of the approximate relation (34).

This implies that the total transport of the ITF depends on the pressure head and on the bottom form stress; on the internal pressure head; and on transports Q_{IO}, Q_{MC}, Q_{NECC}, and Q_{NGCC}. Now we see that the same relation is true for "close" solutions (the Type IIA/B experiments). This confirms the robustness of the relation (34) in Part I.

4. The seasonal variations of the pressure heads and the through-the-ports total transports

In Part I, four proxies were used to quantitatively measure the pressure head. They are the x- and y-components of the resultant of pressure forces acting on the fluid at the external side boundaries (XEPRH and YEPRH); the total work (per unit time) performed by the pressure forces at the four ports (PREWK), and the sea-surface height difference between a point in the Pacific and a point in the Indian Ocean (SSHDIF). In Figure 5 we present the seasonal variation of all four measures of the pressure head for the Type I and the Type IIA/B experiments. All characteristics vary in-phase with each other. The highest values of XEPRH, PREWK, and SSHDIF for both the Type I and Type II experiments occur during the boreal summer when the total transport of the ITF is highest; the lowest during the winter. The Type I values are between the Type IIA and Type IIB values. All values of XEPRH, SSHDIF, and PREWK are negative in accordance with the direction of the ITF (outflow through the IO port). Therefore, the absolute values of these characteristics are larger for the Type IIA experiments and smaller for the Type IIB experiments (relative to the values of the Type I experiment). For the Type IIA experiment |XEPRH| is increased on average approximately by 25%; |SSHDIF|—by 20%; and |PREWK|—by 40%, and by much higher values for the winter. For the Type IIB experiment, |XEPRH| is decreased by 20%; |SSHDIF|—by 16%; and |PREWK|—by 27%, and by much lower values for the winter. The values of YEPRH, however, change sign, although the variation of YEPRH is in-phase with that of XEPRH, SSHDIF, and PREWK. The deviations of |YEPRH| for the Type IIA/B experiments are on the order of 60% relative to that value for the Type I experiment.

The seasonal variations of the total transports through the open ports, Q_{IO}, Q_{MC}, Q_{NECC}, and Q_{NGCC}, are given in Figure 6 (taking into account the appropriate sign). It is clearly seen that the absolute values of all transports are increased for the Type IIA experiment and decreased for the Type IIB experiments (relative to the corresponding value for the Type I experiment). Relative to the values of the Type I experiment, the corresponding values for the Type IIA/B experiments, Q_{MC}, Q_{NECC}, and Q_{NGCC}, change by only 3%–5%. The changes of Q_{IO} for the Type IIA/B experiments, relative to that for the Type I experiment, is more significant; they equal to 16%–19% in the spring, summer, and fall and reach 50% in the winter. Formally this is due to the fact that the variations of Q_{MC}, Q_{NECC}, and Q_{NGCC} are arithmetically added to give more noticeable variation of Q_{IO}, so there is no violation of the mass balance. It is worth noting that the variations of all transports are in-phase.

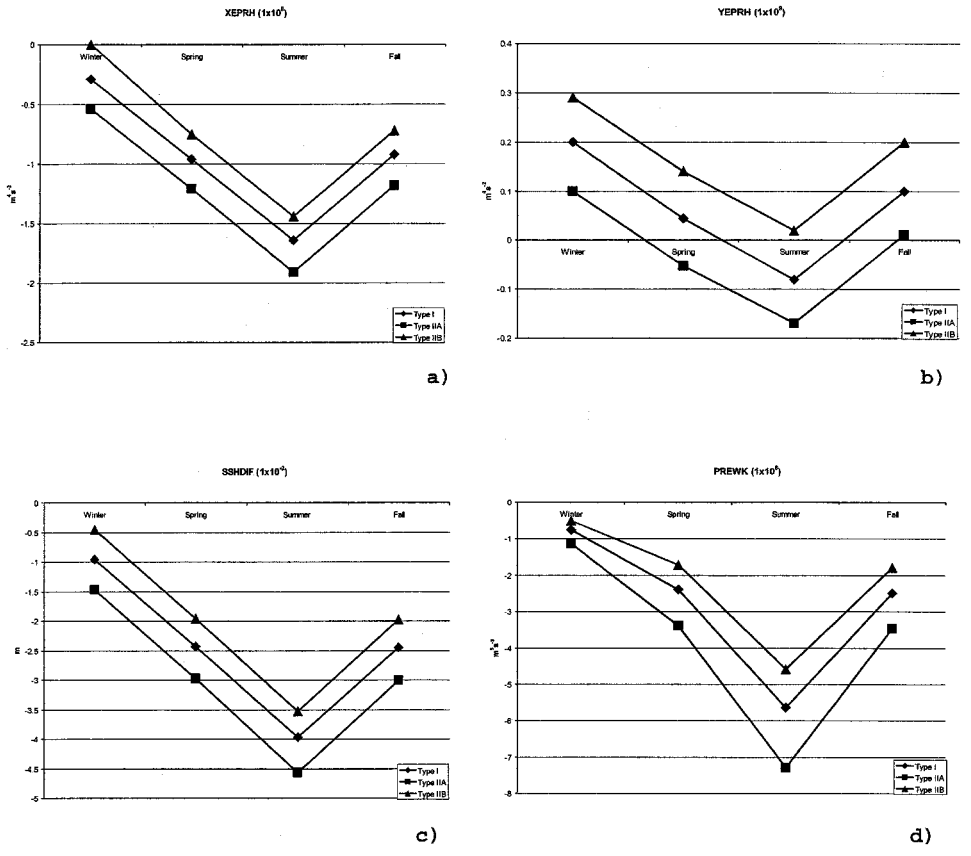

Figure 5. The seasonal variation of the various measures of the pressure head XEPRH (a), YEPRH (b), SSHDIF (c), and PREWK (d) for the Type I and the Type IIA/B experiments.

Note that we failed to make the relative change of Q_{IO}, as small as that of the other port transports. But the relative changes of all the pressure-head measures appear more noticeable as compared to the relative changes of the port transports. That gives an additional point in favor of the conclusion for the lack of the unique relation between the pressure head and the total transport of the ITF.

Finally, we compare the seasonal variations of all measures of the pressure head and the total transport of the ITF for the Type I experiment (with and without local wind stresses) and the Type IIA/B experiments (Fig. 7). All variations are in-phase except for the Type I experiment with wind. When a local wind is included, XEPRH, YEPRH, and WUSURF change similarly; however, the periods of their maximal variations do not coincide. Moreover the variations of SSHDIF, PREWK, and WVSURF are completely out of phase with the variation of the pressure head. If we exclude this case and view Wyrtki's idea

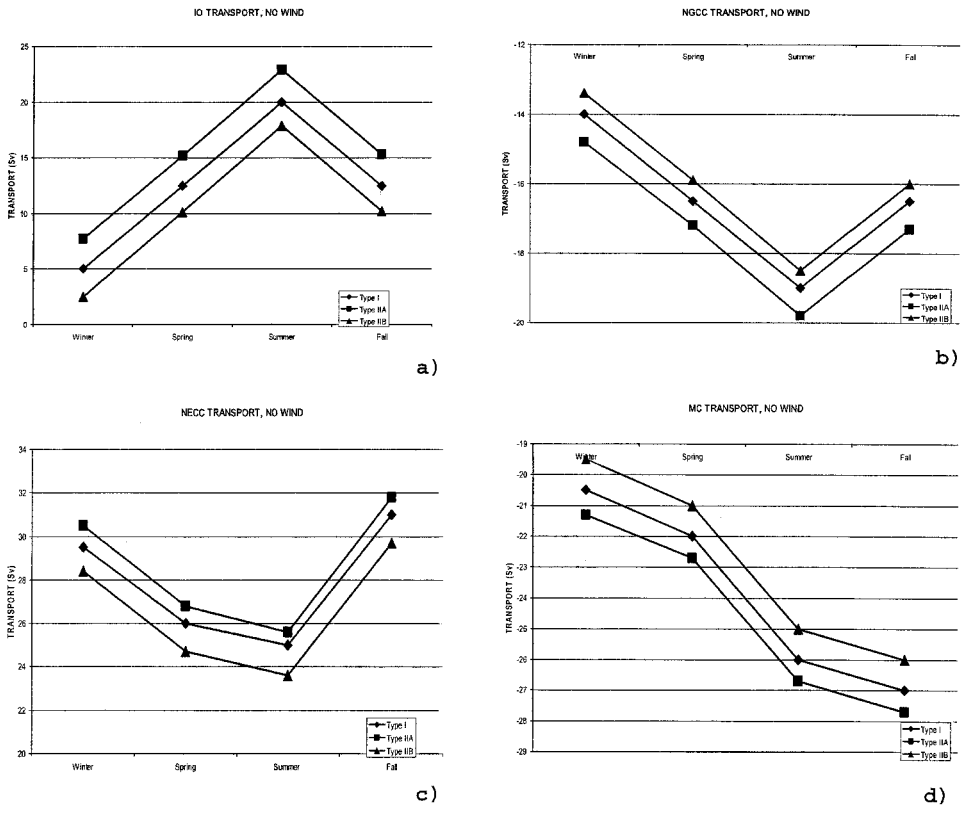

Figure 6. The seasonal variation of the transports at the IO (a), NGCC (b), NECC (c), and MC (d) for the Type I and the Type IIA/B experiments. The inflow transports are positive and the outflow transports are negative.

about the correlation between the pressure head and the total transport of the ITF as an in-phase variation, then the Wyrtki hypothesis appears validated by the present research.

5. Discussion

To study the influence of the Pacific/Indian Ocean pressure difference on the Indonesian Seas circulation we have tried to find solutions with an increased (decreased) pressure at the Pacific open ports and decreased (increased) pressure at the Indian Ocean open port (relative to the solution constructed in the Type I experiment). More specifically, we have tried to increase (decrease) the pressure at the Pacific open ports by a constant value and decrease (increase) the pressure at the Indian Ocean open port by a related constant. If such solutions exist, we will be able to increase (decrease) the pressure difference between the oceans without changing the pressure gradients across the open ports. Then, due to

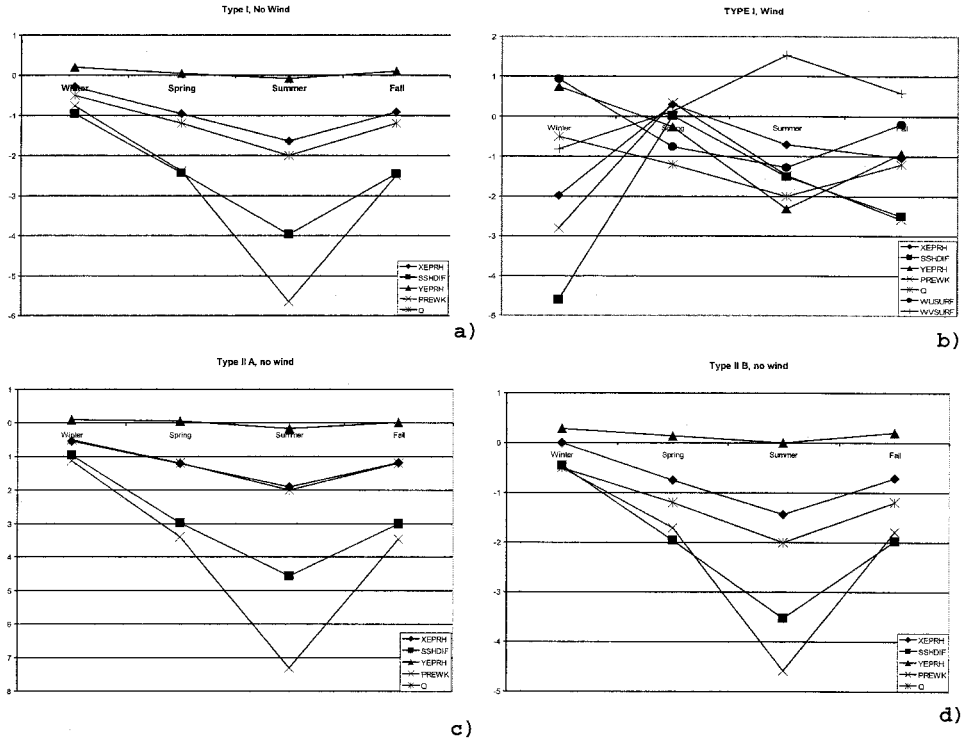

Figure 7. The comparison of the seasonal variation of the (negative) total transport of the ITF, Q (Sv) and different measures of the pressure heads: XEPRH ($m^4\ s^{-2}$), SSHDIF (m), YEPRH ($m^4\ s^{-2}$), PREWK ($m^5\ s^{-3}$), WUSURF and WVSURF ($m^4\ s^{-2}$) for the Type I experiment with no wind (a), the Type I experiment with wind (b), and the Type IIA/B experiments (c and d). In case (b) we consider the components of the wind stress integrated over the model domain.

geostrophy that exists at the entrances of the open ports, it is clear that the total transports through the open ports will not substantially change, including the total transport through the IO port (the total transport of the ITF). Thus, different patterns of Indonesian Seas circulation would exist with sufficiently distinct intra-ocean pressure differences and almost the same total transport of the ITF. In other words, the pressure difference between the Pacific and Indian Ocean would not practically impact the value of the ITF total transport.

We thought that such solutions are dynamically possible. In fact, it seems reasonable to assume that the overall momentum and energy balance relations (1)–(5) will govern such solutions. Then any significant change in the pressure heads (XEPRH and YEPRH) would be balanced by the bottom form stress (XBTS and YBTS) and by the internal pressure heads (XIPRH and YIPRH) thus leading to the small changes of the total transport. Further, any significant change of the PREWK would be balanced by the appropriate

change of HFWRK, which is determined by the velocity gradients rather than by the velocity itself as in the case of the bottom friction.

To construct the Type-II-experiment solutions we reconfigured the regional barotropic model of Part I to specify the sea-surface heights at the open ports, rather than the total transports. Then we introduced the perturbed solutions with the perturbed constant values of the sea-surface height at the open ports.

As the preceding analysis has shown, we managed to find the solutions with noticeable changes in the pressure head and almost the same total transport through the MC, NECC, and NGCC ports. But it appeared that the relative change of the transport through the IO port, exceeded the relative changes for the above-mentioned transports by a factor of 3, being at the same time on average smaller as compared to the relative changes of the pressure head. Why is that?

Figure 8a presents the normal velocities for the Type I and the Type IIA/B experiments at the entrance of each open port for the boreal summer (representative of each season, see Burnett, 2000). Recall that the geostrophic approximation was valid at all open ports except for parts of the NGCC open port where the equator crosses the port, and in the southern boundary of the IO open port where a computational western boundary layer develops (Burnett *et al.,* 2000). It is possible that ageostrophic effects cause the distinction between normal velocities at the port entrance of the Type IIA/B and Type I.

It is not improbable, however, that there are other reasons for the variation of the normal velocities at the port entrance besides the ageostrophic effects. Mathematically the problem corresponding to the Type II experiment appeared to be very complicated and we failed to reach the exact fulfillment of the boundary conditions within the mouth of the ports. We applied the method of a special relaxation to solve the problem (see Appendix B) and obtained an approximate solution with some deviations of the sea-surface heights in the ports from the prescribed values. This is clearly seen in Figure 8b where the boreal summer sea-surface heights are presented (representative of other seasons, see Burnett, 2000); the profiles are not parallel, as they should be for the exact solution (especially for MC and IO ports). It is conceivable that the problem considered has no solution at all and it is possible to find a "close" solution to the one sought only. To illustrate this point consider a flow whose dynamics is such that variations of the pressure along the flow and across the flow are connected (such a flow exists; see, for example, a boundary layer current governed by (15), Part I). Therefore by varying the pressure gradient along the flow we inevitably vary the pressure gradient across the flow. It is clear that the Type IIA/B problem for such a flow has no solution. As to our case, we do not know whether the sought solution exists or not.

Nevertheless we consider the Type IIA/B experiment solutions to be very helpful in studying the two objectives formulated in the introduction of this paper. First, such solutions are interesting per se. Second, they are alternative solutions, closely related to solutions of the Type I experiment. All the conclusions based on the analysis of the Type I

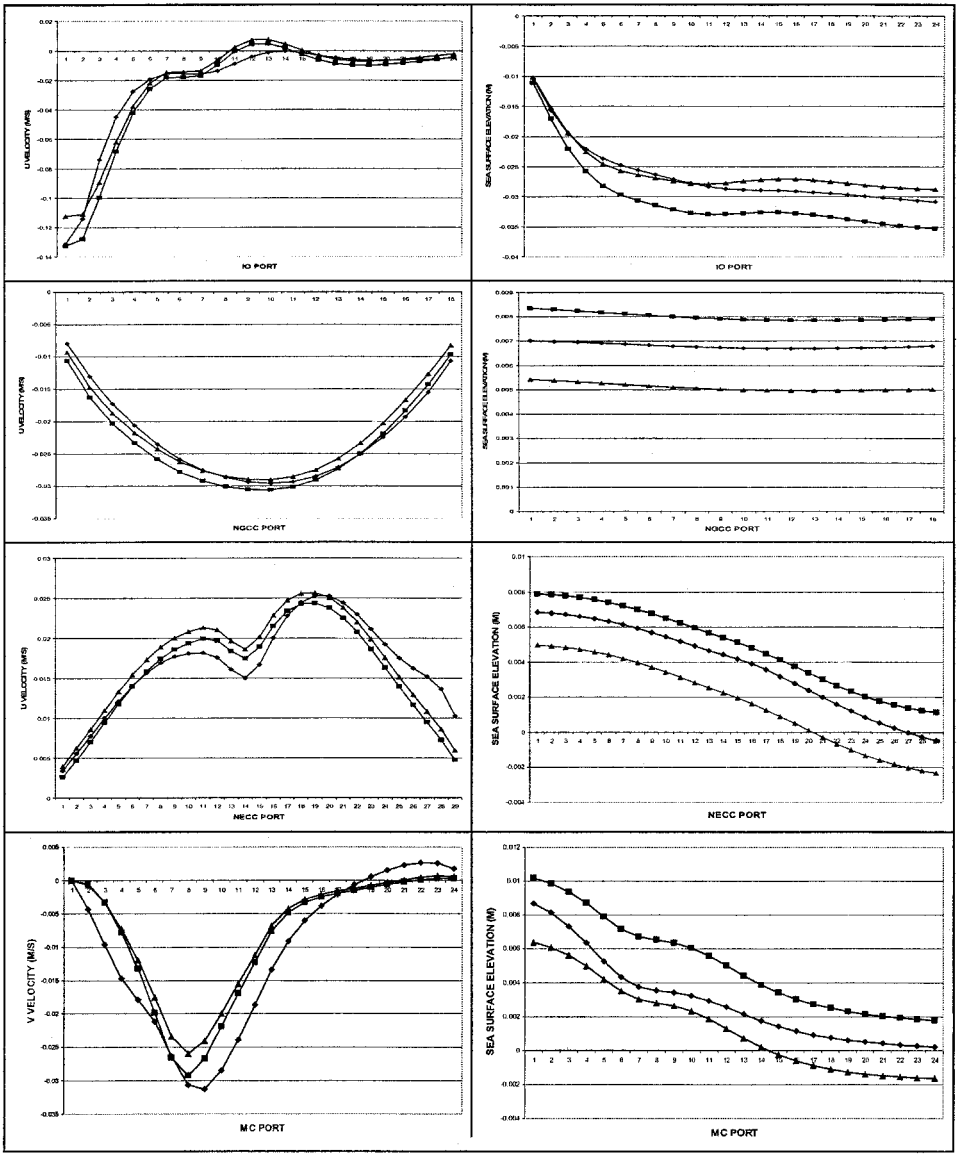

Figure 8. Comparison of the normal velocities at the entrances of the four open ports for the Type I experiment (diamonds), the Type IIA experiment (squares), and the Type IIB experiment (triangles) for the summer (a), and comparison of the corresponding sea surface heights (b). By the entrance of the IO port we imply grid points I = 5, J = 26, . . . , 49; Similarly for other ports.

experiments are valid for these solutions as well. We have shown also that these solutions will give additional credence to the conclusion for the lack of a unique relation between the pressure heads and the value of the total transport of the ITF.

6. Conclusion

Both of the objectives formulated in the Introduction have been met. First, the solutions of the Type IIA/B experiments have been constructed and are considered to be perturbations of the solution of the Type I experiment. We have shown the validity of the approximate relation (34) from Part I for the solutions of the Type IIA/B experiments. In other words, we confirmed that the total transport of the ITF depends on the bottom form stress; on the internal pressure head; on the total transports through the Mindanao, North Equatorial Counter Current, and New Guinea Coastal Current ports and on the pressure head itself. This is true not only for the solution of the Type I experiment but for the "close" solutions of the Type IIA/B experiments as well. Through these experiments we were able to demonstrate the robustness of the relation (34), Part I. Moreover the comparison of the relative changes of all of the measures of the pressure head and the transports through the open ports showed the possibility of the existence of different Indonesian Seas circulation patterns with distinct inter-oceans pressure differences and almost the same total transport of the ITF. This point gives additional credence to our main conclusion.

Second, we qualitatively confirmed the hypothesis by Wyrtki (1987) about the correlation between the seasonal variation of the pressure head and the total transport of the ITF. We viewed the Wyrtki result as the in-phase variations of the pressure head and the total transport of the ITF. Potemra *et al.* (1997) and Lebedev and Yaremchuk (2000) also support the pioneering result by Wyrtki (1987) with detailed analyses of the seasonal variations of the total transport and the sea-surface height differences on the Pacific and Indian Ocean sides of the Indonesian Seas area. This was confirmed for all four measures of the pressure head. Yet we note that the value of the total transport by itself is not uniquely determined by any of the four measures of the pressure head introduced.

The results of the Type I experiments with the local wind effects cannot be considered as supporting this conclusion. Some of the measures of the pressure heads are varied out of phase while compared with the total transport. We think that this case needs more investigation within the baroclinic model that is now in progress.

Acknowledgments. First of all, we would like to thank George Veronis for a very productive discussion that resulted in the considerable clarification of several points of the paper. The authors gratefully acknowledge helpful advice from H. Hurlburt and D. Nechaev on different aspects of the paper. The criticism of our three reviewers was very useful and allowed us to substantially modify the initial outline of the material. V. Kamenkovich was supported by NSF

grants OCE 96-33470 and OCE 01-18200. W. Burnett was supported by U.S. Navy funds. A. Gordon was supported by NSF grants OCE 00-99152 and OCE 96-33470. G. Mellor was supported by NSF grant OCE 96-33470. The model analysis was supported by the Department of Defense's Major Shared Resource Center. The Naval Oceanographic Office Visualization Laboratory prepared the color graphics.

APPENDIX A

Frequently used terms

BFWK—the total work performed by the bottom friction forces (per unit time), see (40) Part I.

HFWK—the total work performed by the horizontal friction forces (per unit time), see (40) Part I.

ITF—Indonesian Throughflow

IO port—Indian Ocean open port (outflow)

MC port—Mindanao Current open port (inflow)

NECC port—North Equatorial Counter Current open port (outflow)

NGCC port—New Guinea Coastal Current open port (inflow)

PREWK—minus the total work performed by the pressure forces at the four ports (per unit time), see (40) Part I.

Q_{IO}—total transport through the IO port.

Q_{MC}—total transport through the MC port

Q_{NECC}—total transport through the NECC port

Q_{NGCC}—total transport through the NGCC port.

SSHDIF—the sea-surface height at the mouth of the IO port (I = 5, J = 49) minus the sea-surface height at the mouth of the MC port (I = 166, J = 246). Introduced to imitate Wyrtki's characteristic.

TENER—The sum of kinetic and potential energies integrated over the total fluid volume (see (40), Part I)

Type I experiment—Experiment with normal and tangential velocities prescribed at the open ports and no slip boundary conditions at the closed part of the boundary

Type II experiment—Experiment with sea-surface-heights and tangential velocities prescribed at the open ports and no slip boundary conditions at the closed part of the boundary

Type IIA experiment—Experiment with the boundary sea-surface-height values equal to the corresponding output values from the Type I experiment plus a constant perturbation of 2.5 mm at the MC, NECC, and NGCC open ports in the Pacific.

Type IIB experiment—the same as in Type IIA except minus a constant perturbation of 2.5 mm at the Pacific open ports.

WUSURF—the x-component of the wind stress integrated over the model domain
WVSURF—the y-component of the wind stress integrated over the model domain
XCOR—the x-component of the Coriolis acceleration integrated over the total fluid volume (see (28) Part I)
XBTS—the x-component of the resultant of pressure forces acting on the fluid at the bottom (see (30) Part I)
XEPRH—the x-component of the resultant of pressure forces acting on the fluid at the external side boundaries (see (31), Part I)
XIPRH—the x-component of the resultant of pressure forces acting on the fluid at the internal side boundaries (see (32), Part I)
XPGRD—the x-component of the pressure gradient integrated over the total fluid volume (see (28) Part I)
XPRH—the x-component of the resultant of pressure forces acting on the fluid at the side boundaries of the domain, both external and internal (see (30), Part I)
YCOR—the y-component of the Coriolis acceleration integrated over the total fluid volume (see (35) Part I)
YBTS—the y-component of the resultant of pressure forces acting on the fluid at the bottom (see (36) Part I)
YEPRH—the y-component of the resultant of pressure forces acting on the fluid at the external side boundaries (see (37), Part I)
YIPRH—the y-component of the resultant of pressure forces acting on the fluid at internal side boundaries (see (38), Part I)
YPGRD—the y-component of the pressure gradient integrated over the total fluid volume (see (35) Part I)
YPRH—the y-component of the resultant of pressure forces acting on the fluid at the side boundaries of the domain, both external and internal (see (36), Part I)

APPENDIX B

Difference formulation

Refer to Appendix A of Part I (Burnett *et al.,* 2003) for a description of the open port boundary conditions. Consider the IO open port ($I = 1, \ldots, 5$; $26 < J, <49$); other ports are handled similarly. We specify $\eta(2, J)$ and $V(2, J)$; calculate $U(3, J)$ from the x-momentum equation by neglecting the horizontal friction and momentum advection; and set $U(2, J) = U(3, J)$ as computational boundary conditions. A schematic is provided in Fig. B.1.

Relaxation is applied within the open ports to suppress numerical noise following Martinsen and Engedahl (1987). The relaxation procedure for the IO open port takes the form:

$$\eta^{n+1}(I, J) = \alpha(I)\eta^{n+1}(2, J) + (1 - \alpha(I))\tilde{\eta}^{n+1}(I, J) \tag{B.1}$$

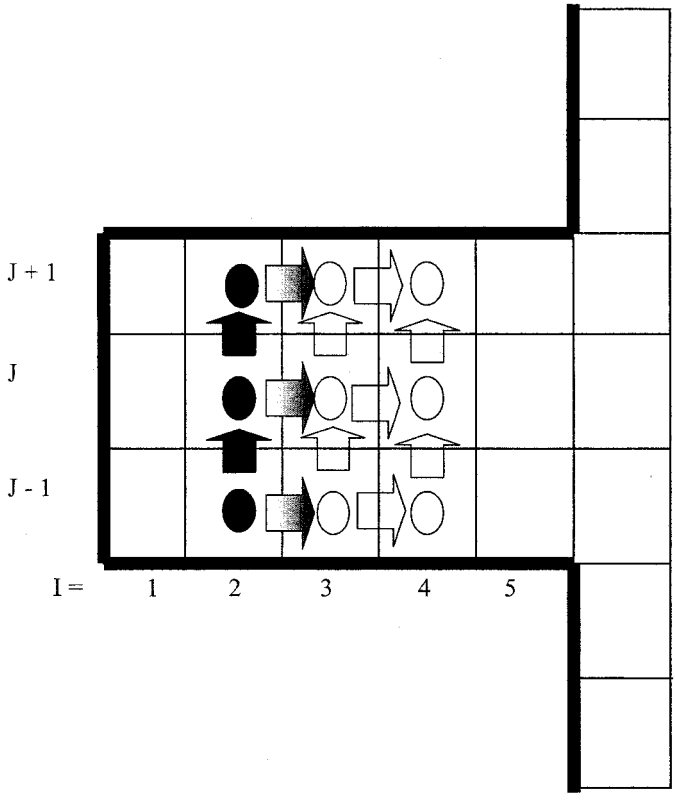

Figure B.1. The schematic of the specified and calculated U, V, and η for the IO port ($26 \leq J \leq 49$) for I = 2; 3; 4 for the Type II experiment. The prescribed sea surface heights $\eta(2, J)$ and tangential velocities $V(2, J)$ are denoted by black arrows and ovals. Normal velocities $U(3, J)$ calculated by neglecting horizontal diffusion and momentum advection (a computational boundary condition) are denoted by partially filled ovals. $U(2, J) = U(3, J)$ is another computational boundary condition, not shown here. Clear arrows and ovals denote variables that are calculated by using the basic equations of the Princeton Ocean Model as in Part I (Burnett *et al.,* 2003).

$$v^{n+1}(I, I) = \alpha(I)v^{n+1}(2, J) + (1 - \alpha(I))\tilde{v}^{n+1}(I, J) \tag{B.2}$$

$$u^{n+1}(I, J) = \alpha(I)u^{n+1}(2, J) + (1 - \alpha(I))\tilde{u}^{n+1}(I, J) \tag{B.3}$$

for I = 3; 4; 5 and $26 \leq J \leq 49$, where $\eta^{n+1}(I, J)$, $u^{n+1}(I, J)$, $v^{n+1}(I, J)$ denote the value at n + 1 time step; $\eta^{n+1}(2, J)$ and $v^{n+1}(2, J)$ are prescribed as boundary conditions while $u^{n+1}(2, J)$ is taken from the boundary condition of the Type I experiment; and $\tilde{\eta}^{n+1}$, $\tilde{u}^{n+1}$, $\tilde{v}^{n+1}$ are calculated from the set of difference equations approximating the basic equations. The relaxation parameter, $\alpha(I)$; I = 3, 4, 5; is equal to 0.028, 0.0028, and 0.00028. Such a

procedure is equivalent to adding Newtonian friction to the basic equations, which in the difference form (corresponding to relation (B.1)) is $K_i\,[\eta^{n+1}(\mathrm{I}, \mathrm{J}) - \eta^{n+1}(2, \mathrm{J})]$, where $K_i = \alpha_i/[(1 - \alpha_i)\Delta t]$, Δt is the time step, and $K(\mathrm{I}) = 0.002, 0.0002$, and 0.00002 for I = 3, 4, 5 (similarly for relations (B.2. and (B.3)). This procedure is analogous for the other ports.

It is important to stress that the physical interpretations from the numerical experiments will be done within the operational domain: I = 5, . . . , 246; J = 2, . . . , 246. Therefore $\eta = \eta(5, \mathrm{J})$, J = 26, . . . , 49; $\eta = \eta(246, \mathrm{J})$, J = 126, . . . , 144; $\eta = \eta(246, \mathrm{J})$, J = 176, . . . , 204; and $\eta = \eta(\mathrm{I}, 246)$, I = 166, . . . , 189 will be considered as physical boundary conditions for the sea surface elevation. The boundary conditions for η specified at I = 2; I = 249; and J = 249 of the corresponding open ports will be referred to as numerical ones.

To check that the outlined approach is working and will provide us with reasonable solutions we ran a Type II experiment with the corresponding Type I experiment output data as boundary conditions at the open ports. The agreement with the Type I experiment was satisfactory.

REFERENCES

Burnett, W. H. 2000. A dynamical analysis of the Indonesian Seas Throughflow. Ph.D. dissertation, Department of Marine Science, University of Southern Mississippi Press, Hattiesburg, MS, 114 pp.

Burnett, W. H., V. M. Kamenkovich, A. L. Gordon and G. L. Mellor. 2003. The Pacific/Indian Ocean pressure difference and its influence on the Indonesian Seas circulation: Part 1—The study with specified total transports. J. Mar. Res., *61,* 577–611.

Burnett, W. H., V. M. Kamenkovich, D. A. Jaffe, A. L. Gordon and G. L. Mellor. 2000. Dynamical balance in the Indonesian Seas circulation. Geophys. Res. Lett., *27,* 2,705–2,708.

Lebedev, K. V. and M. I. Yaremchuk. 2000. A diagnostic study of the Indonesian throughflow. J. Geophys. Res., *105*(C5), 11,243–11,258.

Martinsen, E. A. and H. Engedahl. 1987. Implementation and testing of a lateral boundary scheme as an open boundary condition in a barotropic ocean model. Coastal Eng., *11,* 603–627.

Potemra, J. T., R. Lukas and G. T. Mitchum. 1997. Large-scale estimation of transport from the Pacific to the Indian Ocean. J. Geophys. Res., *102*(C13), 27,795–27,812.

Wyrtki, K. 1987. Indonesian throughflow and the associated pressure gradient. J. Geophys. Res., *92*(C12), 12,941–12,946.

Received: *21 August, 2001;* revised: *9 September, 2003.*